Nanoscale Advances

ROYAL SOCIETY OF CHEMISTRY

MINIREVIEW

View Article Online
View Journal | View Issue

Cite this: *Nanoscale Adv.*, 2022, **4**, 5245

Recent developments in polypyrrole/manganese oxide-based nanocomposites for thin film electrodes in supercapacitors: a minireview

Paresh S. Gaikar,[a] Kedar S. Kadu,[a] Kailas K. Tehare,[b] Gurumeet C. Wadhawa,[e] Sami H. Mahmood *[c] and Trimurti L. Lambat *[d]

Received 23rd September 2022
Accepted 7th November 2022

DOI: 10.1039/d2na00654e

rsc.li/nanoscale-advances

This review article highlights the recent developments in the synthesis and electrochemical performance of polypyrrole/manganese oxide thin-film electrodes synthesized by various chemical methods for supercapacitor applications. In the class of conducting polymers for electrode applications, polypyrrole (Ppy) is considered an important polymer due to its low cost and abundance. Ppy's polymeric composition and structural properties, however, pose stability concerns and have a drawback of a short life cycle over long-term charge–discharge processes, limiting its potential for industrial and commercial utilization. Recently, manganese oxide (MnO_2) has been actively explored as a supercapacitor electrode material due to its low cost, high theoretical specific capacitance and abundance. Ppy/MnO_2 thin film electrodes revealed high specific capacitance and stability, making them excellent candidates for next-generation supercapacitor electrode materials.

1. Introduction

The global economy has relied significantly on the extraction and use of fossil fuel resources such as coal, natural gas, and petroleum. With the increasing demand for fossil fuels, the depletion of fossil fuel resources has produced a slew of economic and societal issues.[1–4] Years ago, the extensive development of diverse energy sources such as hydro, biomass, wind, and tidal energy greatly decreased energy and environmental challenges.[5–7] The produced electric energy is normally stored for redistribution and future use. To accomplish effective energy storage, there was an urgent need to develop a reliable electrochemical energy storage technology, such as a supercapacitor.[8–11] Supercapacitors have a higher energy density than conventional capacitors and a higher power density than batteries. Furthermore, supercapacitors offer high reversibility and long life cycles.[12–16] Supercapacitors are classified into two types based on the electrode materials used and the charge storage mechanisms: (1) electric double-layer capacitors (EDLCs), which use carbon with a large surface area as electrodes[17–19] and (2) pseudo-capacitors, which use electroactive materials such as transition metal oxides or conducting polymers as electrodes.[20–23] In concept, literature evaluations of metal oxide electrodes revealed that these electrodes may exhibit a high specific capacitance and high rate capability. However, one of the metal oxide material's fundamental flaws is its low electrical conductivity. To circumvent this drawback, hybrid supercapacitors were developed by combinations of EDLC materials with conductive polymers or metal oxides. Also, thin films and layered structures of composites were proposed for improvement of the supercapacitor performance. On the other hand, conducting polymers have a lower cost than metal oxides and a higher charge density than carbon.[24–28]

Exhibiting the highest inherent conductivity among any known conducting polymer, Ppy had attracted considerable attention since the monomer (pyrrole) is easily oxidized and is water-soluble. In addition to its high conductivity, Ppy has a strong redox reversibility and environmental stability.[11,29,30] Several Ppy-based products were commercialized including fuel cells, secondary batteries, sensors, supercapacitors, photocatalysts and corrosion prevention compounds.[31–40] Nano-sized materials with a large surface area and porosity could perform admirably as electrode materials for supercapacitors. Furthermore, nanostructured materials such as nanoparticles, nanowires, nanosheets, nanotubes, and nanoribbons show promise for improving electrode electrical conductivity.[41,42] However, Ppy's polymeric composition and structural features cause issues with stability and loss in life cycle during long-term charge–discharge processes which limit its performance in supercapacitors. Because of their strong electrochemical

[a]Department of Physics, Rayat Shikshan Sanstha's, Karmaveer Bhaurao Patil College Vashi, Navi Mumbai 410206, Maharashtra, India
[b]Department of Physics, Dr. Ajeenkey D. Y. Patil School of Engineering, Lohegaon, Pune 412105, Maharashtra, India
[c]Department of Physics, The University of Jordan, Amman 11942, Jordan. E-mail: s.mahmood@ju.edu.jo
[d]Department of Chemistry, Manoharbhai Patel College of Arts, Commerce & Science, Deori, 441901, Dist-Gondia, Maharashtra, India. E-mail: lambatges@gmail.com
[e]Department of Chemistry, Rayat Shikshan Sanstha's, Karmaveer Bhaurao Patil College Vashi, Navi Mumbai 410206, Maharashtra, India

activity, metal oxides have a convenient shape that provides great performance, but they also have the issue of aggregation. The formation of metal oxide aggregates during the manufacture of active electrode materials is greatly impeded by the presence of a structured Ppy film.[11] For supercapacitor electrode materials, conducting polymers and metal oxides/hydroxides have emerged as promising electrode materials.[43] MnO_2 demonstrated promising potential as a pseudocapacitor material with a high specific capacitance of ~1233 F g^{-1}.[44] Consequently, the synergetic action of Ppy and MnO_2 nanoparticles in Ppy/MnO_2 nanocomposites was anticipated to be fruitful for supercapacitor applications.[45,46] Accordingly, we have witnessed an exponential growth in the number of publications related to MnO_2 supercapacitor applications since the beginning of this century as illustrated in Fig. 1 (data collected from Google Scholar). The exponential fit (dashed line in Fig. 1) indicates that the number of publications increased from an insignificant number at the beginning of this century up to 136 articles per year in 2017, and is expected to be around 740 articles per year in 2024.

Since the earliest days of nanoscience, the production of nanomaterials in large quantities at a reasonable price has faced several challenges. Specifically, in an attempt to develop effective electrode materials, many chemical and physical approaches have been employed to design a nanocomposite of Ppy/MnO_2 for supercapacitor applications.[31,47] In comparison to physical approaches, solution chemical synthesis is a simple and alternative synthesis strategy for producing the Ppy/MnO_2 nanocomposite with desirable morphology and improved productivity. Solution-based synthesis methods include hydrothermal synthesis, electrodeposition, chemical bath deposition, polymerization deposition, sol–gel method, and others.[48,49] Solution-based synthesis routes do not require expensive equipment or high vacuum, and they are often simple to process and carry out in moderate circumstances with lower temperatures.[48] However, each solution-based synthesis process has its own set of benefits and drawbacks, and accordingly different scenarios were adopted to complement or collaborate with one another to produce sophisticated nanomaterials.[48] In this minireview, we intend to highlight the commonly used chemical methods for the synthesis of Ppy/MnO_2 nanocomposite electrode materials for supercapacitor applications and summarise the most important results of a two-decade research study in this field.

2. Electrodeposition synthesis of Ppy/MnO_2 nanocomposites

Electrochemical methods exhibit distinct principles and flexibility in controlling the sample structure and shape. Among these, electrodeposition involves electron transport and phase change redox processes. This technique is an excellent approach for fabricating nanostructured films with varied morphologies due to the flexibility of selecting the electrode surface and controlling the appropriate deposition solution and experimental conditions. Electrodeposition creates films or coatings instead of powders for batteries and supercapacitors. Methods of electrodeposition include potentiostatic mode, galvanostatic mode, and potentiodynamic mode.

Chen *et al.* described the electrodeposition process that was employed to synthesize extremely flexible MnO_2/Ppy composite electrodes on carbon cloth (CC) as illustrated in Fig. 2.[50] Electrodeposition typically employs a platinum wire counter electrode and a saturated calomel electrode as a reference electrode. An aqueous solution of 0.5 M $Mn(CH_3COO)_2$ and 0.1 M Na_2SO_4 was used for the electrodeposition of MnO_2 on CC (MnO_2/CC) in a three-electrode system at a static potential of 0.92 V. The second stage involved the electrodeposition of Ppy on the MnO_2/CC samples at a static potential of 0.8 V using an electrolyte of 0.1 M $NaClO_4$ and 0.2% (v/v) Ppy. The produced flexible layered composite electrode exhibited a high specific capacitance of 325 F g^{-1} at a current density of 0.2 A g^{-1}, and a high rate capability with a capacitance retention of 70% at

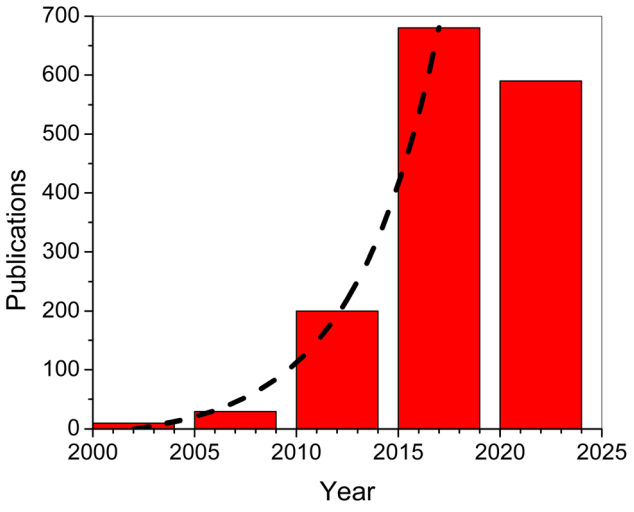

Fig. 1 Number of publications per 5 year period (based on Google Scholar records). The dashed line is an exponential fit.

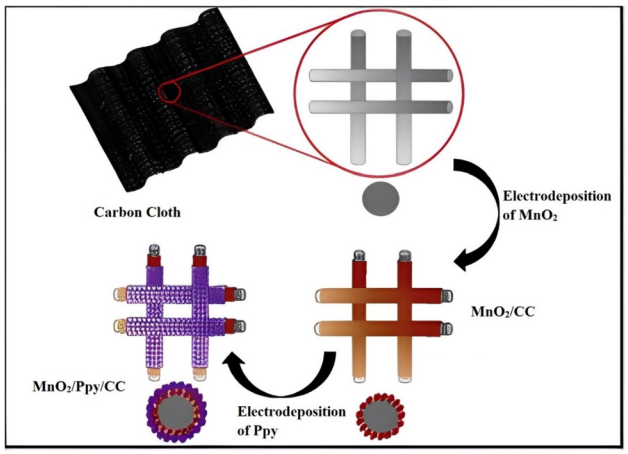

Fig. 2 Schematic view of the fabrication process of the flexible Ppy/MnO_2 composite electrode. Reproduced from ref. 50 with permission from Elsevier, Copyright @ 2016.

a current density of 5.0 A g^{-1}. Over 1000 galvanostatic charge–discharge cycles at a current density of 1 A g^{-1}, it retained 96% of its initial specific capacitance. This work demonstrated the feasibility of developing robust and cost-effective flexible nanocomposite electrodes with high electrochemical performance. The high performance was attributed to an improvement in ion and electron transport properties and efficient functioning of active electrode materials.

Sulaiman *et al.* designed and fabricated a layer-by-layer (LBL) composite of Ppy/graphene oxide/multi-walled carbon nanotube| Ppy/MnO_2 (PGM|PMnO_2) potentiostatically at 0.8 V for 10 min on an ITO substrate. Fig. 3 shows a SEM image and a high resolution TEM image of the as-prepared Ppy/MnO_2 film by other related methods. The LBL composite's synergistic impact between its layers resulted in an increase in the specific capacitance (up to ~756 F g^{-1}) and improvement of the specific energy and specific power in a supercapacitor operating at 1.5 A g^{-1}. In addition, the LBL composite electrode exhibited excellent cycle stability with a low equivalent series resistance of (40.01 Ω).[45] This electrode design exhibited superior performance compared to both PGM and PMnO_2 electrodes, and was proposed as a potential electrode for future generation supercapacitors. A disadvantage of this design, however, is the complexity of the electrode structure, and the work involved in its fabrication.

3. Hydrothermal synthesis of Ppy/MnO_2 nanocomposites

Hydrothermal synthesis is one of the well-known solution-based synthesis processes that is widely utilized for synthesizing different nanomaterials with tailored sizes and morphologies. In hydrothermal synthesis, water is used as the reaction medium and the reaction takes place in a sealed vessel at a temperature normally above 100 °C. Autoclave pressure is influenced by factors such as the volume of liquid inside the vessel and the concentration of salts in the solution. Depending on the vapor pressure of the primary components in the reaction, low-pressure or high-pressure conditions can be tuned to modify the morphology of the final product.

Deyan He and colleagues developed a Ppy-assisted 3D flexible macroporous graphene foam@MnO_2 nanoparticle composite electrode.[51] A 0.03 M $KMnO_4$ solution was prepared and transferred into a stainless-steel autoclave lined with Teflon. The autoclave was sealed and kept at 60 °C for 80 minutes after loading the electrodeposited Ppy/GO samples. Finally, de-ionized water was used to wash and dry the sample at 60 °C. The GF@Ppy@MnO_2 nanoparticle composite electrode exhibited a high specific capacity of 600 F g^{-1} at a current density of 1 A g^{-1}. Furthermore, the tests revealed that more than 92% of the original capacity was retained after 5000 cycles at 30 A g^{-1}. The superiority of the designed layered nanocomposite electrode is demonstrated by the cyclic voltammetry curves. Furthermore, fully symmetric GF@Ppy@MnO_2// GF@Ppy@MnO_2 was designed and tested, and gave a maximum power density of 13 kW kg^{-1} and a maximum energy density of 28 W h kg^{-1}.

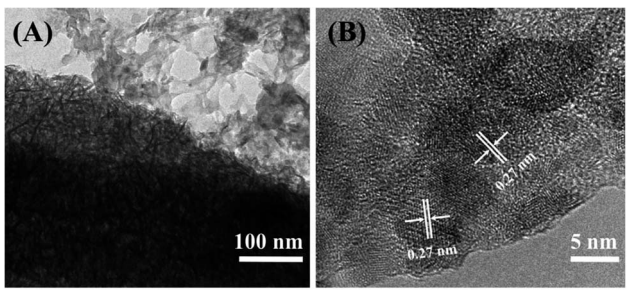

Fig. 3 (A) TEM image of the Ppy/MnO_2 nanocomposite; (B) high-resolution TEM image of the Ppy/MnO_2 nanocomposite. Reproduced from ref. 50 with permission from Elsevier, Copyright @ 2016.

4. Sonochemical synthesis of Ppy/MnO_2 nanocomposites

Unique materials may be made using high-intensity ultrasound, which also offers a novel approach for the production of well-known materials without the need for excessive heat, pressure, or time. Sonochemistry, or the creation or alteration of nanomaterials by ultrasonic irradiation, is the result of a combination of processes. Cavitation, the creation of bubbles in a solution to produce a radical species, is the sonification mechanism. When the bubbles reach their maximum size in the solution they burst, releasing great heat and pressure. As a result, chemical bonds are broken, leading to the generation of free radicals.[52–54] Sonochemical methods are used to fabricate sandwich-like ternary composites. A novel hierarchical structure of (MnO_2, Ppy)/rGO was realized by integrating the multifunctional MnO_2 and Ppy particles with reduced graphene oxide (rGO) nanosheets (Fig. 4). This ternary layered composite structure demonstrated superior electrochemical performance over the constituent materials and their binary composites. The constituents of the conductive sandwich network perform synergistically to enhance the capacitive performance. At a current density of 0.25 A g^{-1} using 1 M Na_2SO_4 electrolyte, a high specific capacitance of 404 F g^{-1} was achieved by this ternary composite. Also, 91% of the initial capacitance was retained after 5000 charge–discharge cycles.[55] The proposed design demonstrated the efficient role of MnO_2 in improving the capacitive performance with a high cycling stability of the electrode.

5. Polymerization synthesis of Ppy/MnO_2 nanocomposites

Metal and metal oxide nanoparticles are dispersed in polymer-supported nanoparticle composites *in situ* and ex-situ. Still, the morphology and physical arrangement of the polymeric material can vary greatly, from spherical beads to granules, membranes, fibers, and other shapes (Fig. 5).[56] Even though the polymer and metal/metal oxide nanoparticles retain their intrinsic characteristics in polymer-supported nanocomposites,

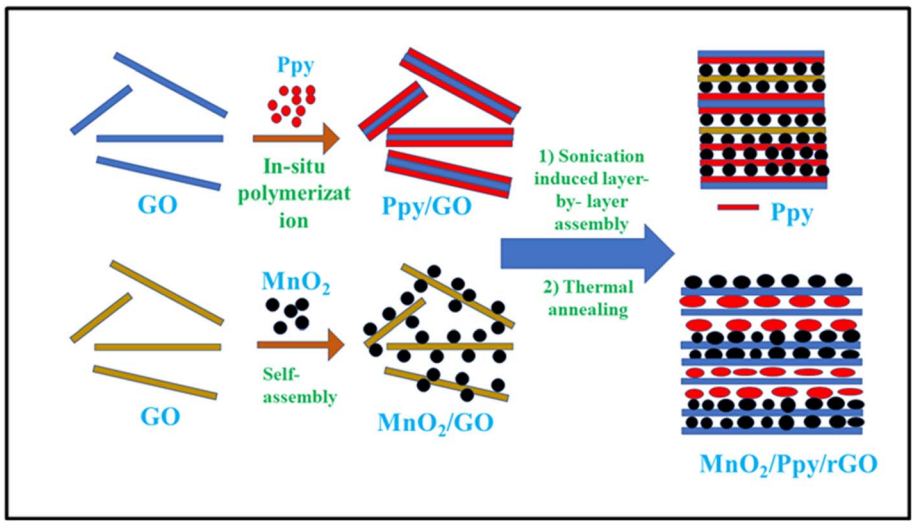

Fig. 4 Schematic diagram of formation of (MnO_2, Ppy)/rGO composites.

these can be modified to improve the overall quality in numerous ways.[57]

The improved electrochemical performance of the fabricated freestanding flexible electrode was attributed to the reduction of the diffusion distance of the electrolyte ions in the charge/discharge process, whereas the strong adhesion between MnO_2 and graphene foam improved the cycling stability (Fig. 6).[58]

To investigate the effect of the pH value of the reactants on the morphology and capacitive performance of the MnO_2/Ppy nanocomposite, solutions of 0.5 M pyrrole, 0.01 M *p*-toluenesulfonate, and 0.03 M $KMnO_4$ were mixed and reacted *in situ* to form nanocomposites with compact sheet, fibrous–porous, and granular morphologies.[56] The pH value of the solution mixture was adjusted by using H_2SO_4. The final solution was stirred for 60 min at room temperature. The MnO_2/Ppy nanocomposite was centrifuged, rinsed with DI water, and dried at 60 °C. The working electrode was developed by dispersing MnO_2/Ppy nanocomposite powder, activated carbon, and PVDF in an *N*-methyl pyrrolidinone solution. The slurry was pressed over 1 cm^2 nickel foam and dried overnight at 60 °C. The cyclic voltammetry curves of the MnO_2/Ppy electrodes at a scan rate of 10 mV s^{-1} in 0.5 M Na_2SO_4 electrolyte revealed significant differences depending on the pH value that was adopted in the preparation of the electrode material, and the highest power density was observed at pH 4.0. The specific capacitance increased sharply from 43 F g^{-1} at pH 1.0 up to a maximum value of 312 F g^{-1} at pH 4.0. As the pH value increased further, the specific gravity decreased slowly (and almost linearly) to ~200 F g^{-1} at pH 7.8. The electrochemical performance of the porous MnO_2/Ppy nanocomposite was further evaluated for a symmetric supercapacitor made from a material prepared at pH 4.0. The symmetric supercapacitor exhibited a specific capacitance per unit mass of one electrode of 142 F g^{-1} at a scan

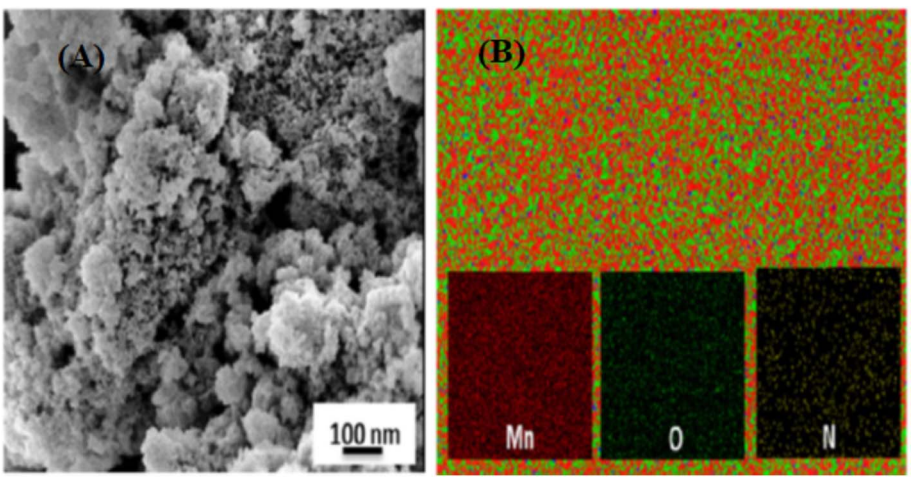

Fig. 5 (A) FESEM image and (B) elemental map of the MnO_2/Ppy nanocomposite. Reproduced from ref. 56 with permission from Elsevier, Copyright @ 2015.

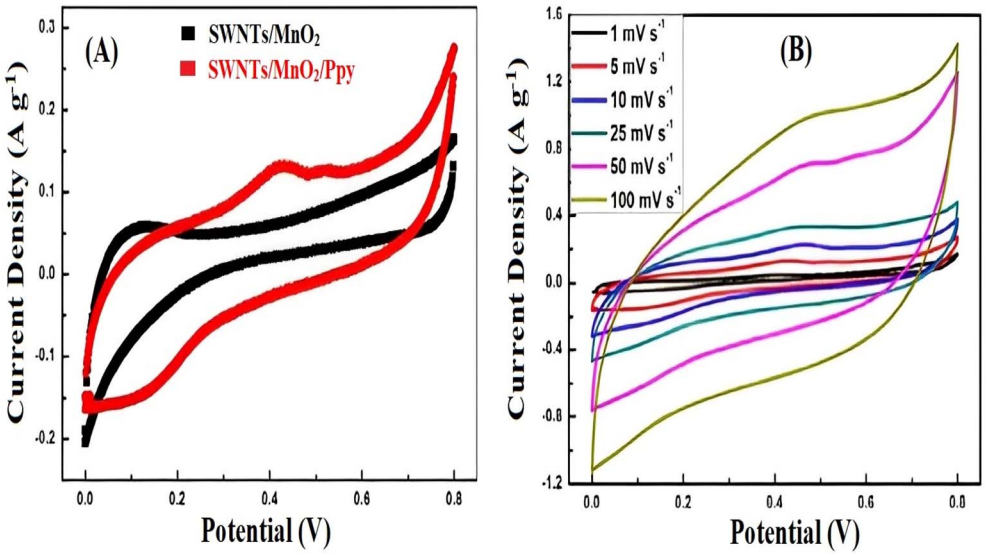

Fig. 6 (A) Comparison of the CV curves of single-walled nanotubes (SWNTs)/MnO_2 and SWNTs/MnO_2/Ppy at a scan rate of 5 mV s^{-1} (B) SWNTs/MnO_2/Ppy electrode CV curves at various scan rates. Reproduced from ref. 58 with permission from Elsevier, Copyright @ 2014.

rate of 25 mV s^{-1} as obtained from the CV curves, which was consistent with the value of 136 F g^{-1} obtained from the galvanostatic charge/discharge curve at a current density of 0.25 A g^{-1}. Furthermore, the symmetric supercapacitor exhibited excellent capacitance retention of 93.2% after 1000 charge/discharge cycles (Fig. 7).[56] This work elucidated the possibility of fabricating efficient electrode structures with tunable morphologies simply by adjustment of the pH value. The electrolyte accessibility is enhanced by the porous nature of the electrode active material, which is facilitated by the high surface activity.

De Oliveira *et al.* designed core/shell structures of multi-walled carbon nanotubes (MWCNT@MnO_2@Ppy) by a chemical polymerization method. According to the described procedure, 50 mg of MWCNT@MnO_2 composite was added to a 30 mL of 5 mM aqueous solution of sodium dodecyl sulfate, which was subsequently stirred vigorously for 20 minutes. Then 0.21 mL of pyrrole was introduced into the solution, and this mixture was stirred at 2 °C for 5 minutes. After this, 50 mL of 0.06 M APS aqueous solution was added dropwise to the solution at 2 °C while stirring for 2 hours. The filtered powder was dried overnight at 70 °C. Pellets of 13 mm diameter were then obtained by pressing 50 mg of the powder under 20 kN. The pellets and separator were then impregnated by the electrolyte by soaking in 1 M aqueous solution of KCl overnight. The concentration of the MWCNT in the composite influenced the charge transfer mechanism and the dielectric response of the composite, and resulted in significant variations in the

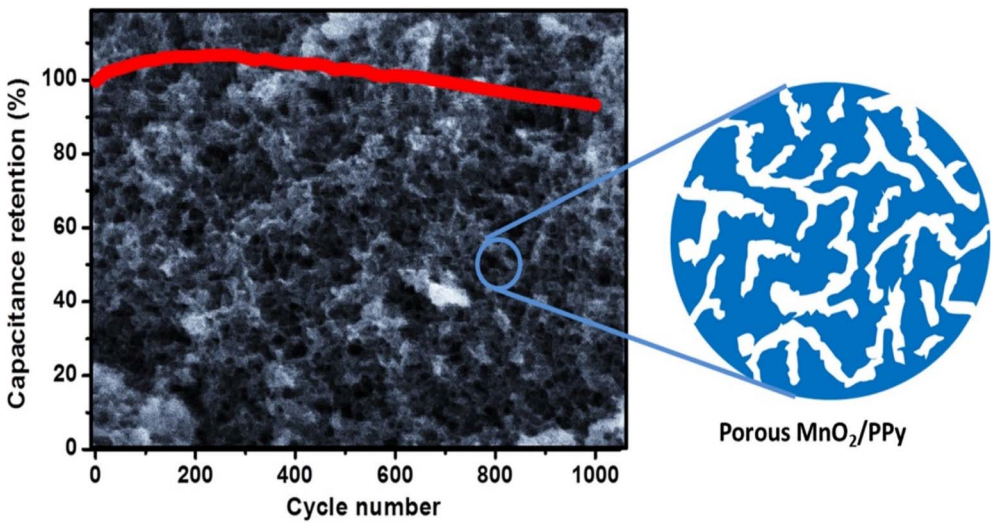

Fig. 7 Cycling stability of the fabricated symmetric MnO_2/Ppy supercapacitor device. Reproduced from ref. 56 with permission from Elsevier, Copyright @ 2015.

Table 1 Ppy–MnO_2 composite synthesis method, performance, electrolyte and potential window

Compound name	Method	Performance	Electrolyte	Potential	Reference
Ppy	Electrodeposition	SC 8 mF @ 100 mV s^{-1}	2.0 M KCl	−0.9 to 0.7 V	59
Ppy	Polymerization	SC 400 F g^{-1} @ 100 mV s^{-1}, 80% retention @ 5 mA cm^{-2} for 5000 cycle	0.5 M H_2SO_4	−0.2 to 0.8 V	60
Ppy	Electrodeposition	SC 329 F g^{-1} @ 5 mV s^{-1}	0.5 M H_2SO_4	−0.4 to −0.6 V	61
Ppy	Electropolymerzation	SC 545 F g^{-1} @ 100 mV s^{-1}	1 M $LiClO_4$	−0.4 to 0.4 V	62
Ppy	Electrodeposition	SC 476 F g^{-1} @ 5 mV s^{-1}	0.5 M H_2SO_4	−0.4 to 0.6 V	63
MnO_2	Sonochemical	SC 282 F g^{-1} @ 0.5 mA cm^{-2}	1 M $Ca(NO_3)_2$	0 to 1.0 V	64
MnO_2	Electrodeposition	SC 128 F g^{-1} @ 1 A g^{-1}	1 M Na_2SO_4	0 to 1.0 V	65
MnO_2	Hydrothermal	SC 73.5 F g^{-1} @ 2 mA cm^{-2}	1 M Na_2SO_4	0 to 1.0 V	31
Ppy–MnO_2	Polymerization	SC 272.72 F g^{-1} @ 1 mV s^{-1}	1 M KCl	0 to 0.3 V	66
Graphene foams@ Ppy–MnO_2	Hydrothermal	SC 601 F g^{-1} @ 1 A g^{-1} 92% retained after 5000 cycles @ 30 A g^{-1}	1 M Na_2SO_4	0 to 1.0 V	51
MnO_2/Ppy/reduced graphene oxide	Sonication	SC 404 F g^{-1} @ 0.25 A g^{-1}	1 M Na_2SO_4	−0.4 to 0.6 V	55
Ppy/MnO_2	Electrodeposition	SC 239 F g^{-1} @ 1 A g^{-1}, 86.7% SC retention @ 10 000 cycles	1 M Na_2SO_4	0 to 0.9 V	67
β-MnO_2/Ppy	Polymerization	SC 294 F g^{-1} @ 1 A g^{-1}	1 M Na_2SO_4	0.0 to 1.0 V	44
Ppy/MnO_2	Electrochemical deposition	SC 755.99 F g^{-1} @ 1.5 A g^{-1}	1.0 M KCl	0.0 to 1.0 V	45
Ppy/MnO_2	Electrochemical deposition	13 mF cm^{-2} @ 0.1 mA cm^{-2}, SC 84% retention 5000 CV cycle @ 500 mV s^{-1}	PVA/$LiClO_4$	0 to 8.0 V	11
MnO_2/Ppy	Electrochemical deposition	SC 141.6 F g^{-1} @ 2 mA cm^{-2}	1 M Na_2SO_4	0.0 to 1.0 V	31
Ppy/MnO_2	Electrochemical deposition	Specific energy of 27.2 W h kg^{-1} at 0.85 kW kg^{-1}	1 M Na_2SO_4	−0.8 to 0.0 V	68
Ppy/MnO_x	Electrochemical deposition	343 F g^{-1} @ 100 mV s^{-1}	1 M H_2SO_4	−0.3 to 0.6 V	69
SWNTs@MnO_2/Ppy	Polymerization	SC 353 F g^{-1} @ 0.1 A g^{-1}	1 M Na_2SO_4	0 to 0.8 V	58
α-MnO_2/Ppy	Polymerization	SC 209 F g^{-1} @ 0.5 A g^{-1}	$Ca(NO_3)_2 \cdot 4H_2O$	0 to 1.0 V	47
Ppy/MnO_2 on carbon cloth	Electrochemical deposition	SC 325 F g^{-1} @ 0.2 A g^{-1}	1 M Na_2SO_4	0 to 1.0 V	50
Nanofiber/MnO_2/Ppy	Electrodeposition	SC 409.88 F g^{-1} @ 25 mV s^{-1}	1.0 M KCl	0 to 1.0 V	46
MnO_2/Ppy	Polymerization	SC 312 F g^{-1} @ 10 mV s^{-1}	0.5 M Na_2SO_4	−0.2 to 0.8 V	41
$Ti_3C_2T_x$ and Ppy/MnO_2	Electrophoretic deposition	SC 128 F g^{-1} @ 5 mV s^{-1} 80.7% SC after 5000 cycles @ 1.72 mA cm^{-2}	PVA/H_2SO_4	0 to 1.2 V	70
Nickel metallized nanofibers based MnO_2/Ppy	Electrodeposition	SC 28.48 F g^{-1} @ 50 mV s^{-1}	—	−0.8 to 0 V	71
MnO_2@Ppy	Electrodeposition	SC 141.6 F g^{-1} @ 2 mA cm^{-2}	1 M Na_2SO_4	0 to 1.0 V	31
MnO_2/Ppy@CNT	Electroplating	SC 461 F g^{-1} @ 0.2 A g^{-1}	1 M Na_2SO_4	0 to 0.85 V	72

electrochemical performance of a double layer capacitor structure. The specific capacitance increased sharply with the increase of MWCNTs reaching a maximum value of ~273 F g^{-1} at 300 mg loading of MWCNTs. With a further increase in the MWCNT concentration, the specific capacitance decreased at a slower rate, reaching ~140 F g^{-1} at 500 mg loading. The associated cycling performance test revealed a capacitance retention of ~60% after 300 charge/discharge cycles. The improvement in electrochemical performance of the electrode was attributed to the improved electrical conductivity and increase in the active surface area for charge accumulation in the composite.

Table 1 below summarizes the performance of different electrode materials synthesized by different chemical techniques.

6. Conclusion

Ppy/MnO_2 nanocomposite electrodes exhibit superior supercapacitive electrochemical performance compared to pristine MnO_2 and Ppy electrodes. Several simple and low-cost chemical techniques were successful in producing Ppy/MnO_2 nanocomposites for supercapacitor electrode materials. The supercapacitive properties of Ppy/MnO_2-based electrodes depend critically on the synthesis route and prevailing experimental conditions. However, several challenges are still being faced in the development of supercapacitors for commercialization. The first and most important problem is the low energy density of supercapacitors compared to rechargeable lithium ion batteries. The development of future generation supercapacitors requires improvements in the design and manufacturing technology and the search for new electrolytes and electrode materials with high electrochemical performance. The second problem is associated with the high and instantaneous power output of the supercapacitor, which may have an impact on the load, and disturb the system stability. The third problem is associated with the high current during charge/discharge processes, where overcharging may have a negative impact on the capacitor life, and consistency of the voltage across capacitors connected in series is crucial. And the

fourth problem is connected to industrial standardization to ensure low cost and green recycling and disposal of scrap. With the rapidly increasing interest in Ppy/MnO_2-based materials for supercapacitor applications, there is hope to pave ways for future developments of high-performance supercapacitors to mitigate environmental and energy-demand challenges.

Conflicts of interest

There are no conflicts to declare.

References

1 S. Maria, M. Pandey, D. Bhattacharjya and B. K. Saikia, *J. Energy Storage*, 2022, **52**, 104938.
2 S. L. Gaikwad, A. P. Angre, V. A. Naik, J. G. Pargaonkar, P. A. Patil, K. V. Chandekar, A. U. Chavan and P. S. Gaikar, *Mater. Today: Proc.*, 2021, **43**, 2663–2667.
3 S. Singh, R. K. Sahoo, N. M. Shinde, J. M. Yun, R. S. Mane and K. H. Kim, *Energies*, 2019, **12**, 3320.
4 Z. S. Iro, C. Subramani and S. S. Dash, *Int. J. Electrochem. Sci.*, 2016, **11**, 10628–10643.
5 P. Gaikar, S. P. Pawar, R. S. Mane, M. Nuashad and D. V. Shinde, *RSC Adv.*, 2016, **6**, 112589–112593.
6 Y. Wang, L. Zhang, H. Hou, W. Xu, G. Duan, S. He, K. Liu and S. Jiang, *J. Mater. Sci.*, 2020, **561**(56), 173–200.
7 P. S. Gaikar, S. T. Navale, V. V Jadhav, P. V Shinde, D. P. Dubal, P. R. Arjunwadkar, F. J. Stadler, M. Naushad, A. A. Ghfar and R. S. Mane, *Electrochim. Acta*, 2017, **253**, 151–162.
8 P. S. Gaikar, A. P. Angre, G. Wadhawa, P. V. Ledade, S. H. Mahmood and T. L. Lambat, *Curr. Res. Green Sustainable Chem.*, 2022, **5**, 100265.
9 M. Rajesh, C. J. Raj, R. Manikandan, B. Chul, S. Yeup and K. Hyun, *Mater. Today Energy*, 2017, **6**, 96–104.
10 N. M. Shinde, P. V. Shinde, R. S. Mane and K. Ho Kim, *Renewable Sustainable Energy Rev.*, 2021, **135**, 110084.
11 W. A. Haider, L. He, H. A. Mirza, M. Tahir, A. M. Khan, K. A. Owusu, W. Yang, Z. Wang and L. Mai, *RSC Adv.*, 2020, **10**, 18245–18251.
12 M. Vijayakumar, A. B. Sankar, D. S. Rohita, T. N. Rao and M. Karthik, *ACS Sustainable Chem. Eng.*, 2019, **7**, 17175–17185.
13 S. Jadhav, P. D. Donolikar, N. R. Chodankar, T. D. Dongale, D. P. Dubal and D. Patil, *J. Solid State Electrochem.*, 2019, **23**, 3459–3465.
14 R. Farzana, K. Hassan and V. Sahajwalla, *Sci. Rep.*, 2019, **9**, 8982.
15 W. Zhou, J. Zhang, T. Xue, D. Zhao and H. Li, *J. Mater. Chem.*, 2008, **18**, 905–910.
16 D. Ni, Y. Chen, H. Song, C. Liu, X. Yang and K. Cai, *J. Mater. Chem. A*, 2019, **7**, 1323–1333.
17 G. Shimoga, R. R. Palem, D. S. Choi, E. J. Shin, P. S. Ganesh, G. D. Saratale, R. G. Saratale, S. H. Lee and S. Y. Kim, *Metals*, 2021, **11**, 1–14.
18 L. Ding, V. Snoeyink, B. Mariñas, Z. Yue and J. Economy, *Environ. Sci. Technol.*, 2008, **42**, 1227–1231.
19 J. Park, H. Jin, M. Kim, H. Jang and M. Ko, *J. Mater. Chem. A*, 2022, **10**, 18626–18635.
20 X. Feng, X. Shi, J. Ning, D. Wang, J. Zhang, Y. Hao and Z.-S. Wu, *eScience*, 2021, **1**, 124–140.
21 A. Soam, R. Kumar, C. Mahender, M. Singh, D. Thatoi and R. O. Dusane, *J. Alloys Compd.*, 2020, **813**, 152145.
22 W. J. Zhou, M. W. Xu, D. D. Zhao, C. L. Xu and H. L. Li, *Microporous Mesoporous Mater.*, 2009, **117**, 55–60.
23 S. L. Kadam and S. B. Kulkarni, *Ceram. Int.*, 2018, **44**, 14547–14555.
24 R. B. Ambade, S. B. Ambade, N. K. Shrestha, Y.-C. Nah, S.-H. Han, W. Lee and S.-H. Lee, *Chem. Commun.*, 2013, **49**, 2308–2310.
25 P. Forouzandeh, V. Kumaravel and S. Pillai, *Catalysts*, 2020, **10**, 969.
26 T. S. Mathis, N. Kurra, X. Wang, D. Pinto, P. Simon and Y. Gogotsi, *Adv. Energy Mater.*, 2019, **9**, 1902007.
27 S. Kulandaivalu and Y. Sulaiman, *Energies*, 2019, **12**, 2107.
28 P. S. Gaikar, S. L. Gaikwad, R. K. Mahadule, G. C. Wakde, A. P. Angre, A. S. Bandekar and P. R. Arjunwadkar, *J. Nanoeng. Nanomanuf.*, 2016, **6**, 157–160.
29 N. Li, X. Li, C. Yang, F. Wang, J. Li, H. Wang, C. Chen, S. Liu, Y. Pan and D. Li, *RSC Adv.*, 2016, **6**, 86744–86751.
30 D. P. Dubal, S. H. Lee, J. G. Kim, W. B. Kim and C. D. Lokhande, *J. Mater. Chem.*, 2012, **22**, 3044–3052.
31 A. Bahloul, B. Nessark, E. Briot, H. Groult, A. Mauger, K. Zaghib and C. M. Julien, *J. Power Sources*, 2013, **240**, 267–272.
32 P. Makvandi, S. Iftekhar, F. Pizzetti, A. Zarepour, E. N. Zare, M. Ashrafizadeh, T. Agarwal, V. V. T. Padil, R. Mohammadinejad, M. Sillanpaa, T. K. Maiti, G. Perale, A. Zarrabi and F. Rossi, *Environ. Chem. Lett.*, 2021, **19**, 583–611.
33 M. Das and S. Roy, *Mater. Sci. Semicond. Process.*, 2021, **121**, 105332.
34 L. Al-Mashat, C. Debiemme-Chouvy, S. Borensztajn and W. Wlodarski, *J. Phys. Chem. C*, 2012, **116**, 13388–13394.
35 T. Osaka, T. Momma, H. Ito and B. Scrosati, *J. Power Sources*, 1997, **68**, 392–396.
36 P. Geng, S. Cao, X. Guo, J. Ding, S. Zhang, M. Zheng and H. Pang, *J. Mater. Chem. A*, 2019, **7**, 19465–19470.
37 M. K. Zadeh, M. Yeganeh, M. T. Shoushtari and A. Esmaeilkhanian, *Synth. Met.*, 2021, **274**, 116723.
38 M. B. González and S. B. Saidman, *Corros. Sci.*, 2011, **53**, 276–282.
39 X. Yuan, X. L. Ding, C. Y. Wang and Z. F. Ma, *Energy Environ. Sci.*, 2013, **6**, 1105–1124.
40 Y. Li, S. Yan, X. Jia, J. Wu, J. Yang, C. Zhao, S. Wang, H. Song and X. Yang, *Appl. Catal., B*, 2021, **287**, 119926.
41 K. N. Dinh, Q. Liang, C. F. Du, J. Zhao, A. I. Y. Tok, H. Mao and Q. Yan, *Nano Today*, 2019, **25**, 99–121.
42 M. Osada and T. Sasaki, *Adv. Mater.*, 2012, **24**, 210–228.
43 G. A. Snook, P. Kao and A. S. Best, *J. Power Sources*, 2011, **196**, 1–12.
44 J. Zang and X. Li, *J. Mater. Chem.*, 2011, **21**, 10965–10969.
45 S. Kulandaivalu, M. N. Mohd Azahari, N. H. N. Azman and Y. Sulaiman, *J. Energy Storage*, 2020, **28**, 101219.

46 M. A. A. Mohd Abdah, N. Abdul Rahman and Y. Sulaiman, *Ceram. Int.*, 2019, **45**, 8433–8439.
47 S. Shivakumara and N. Munichandraiah, *J. Alloys Compd.*, 2019, **787**, 1044–1050.
48 X. Xia, Y. Zhang, D. Chao, C. Guan, Y. Zhang, L. Li, X. Ge, I. Inguez Bacho, J. Tu and H. J. Fan, *Nanoscale*, 2014, **6**, 5008.
49 L. Qiao and M. T. Swihart, *Adv. Colloid Interface Sci.*, 2017, **244**, 199–266.
50 X. Fan, X. Wang, G. Li, A. Yu and Z. Chen, *J. Power Sources*, 2016, **326**, 357–364.
51 T. Qin, B. Liu, Y. Wen, Z. Wang, X. Jiang, Z. Wan, S. Peng, G. Cao and D. He, *J. Mater. Chem. A*, 2016, **4**, 9196–9203.
52 R. F. Elsupikhe, K. Shameli, M. B. Ahmad, N. A. Ibrahim and N. Zainudin, *Nanoscale Res. Lett.*, 2015, **10**, 1–8.
53 A. Hassanjani-Roshan, M. R. Vaezi, A. Shokuhfar and Z. Rajabali, *Particuology*, 2011, **9**, 95–99.
54 X. Hangxun, B. W. Zeiger and K. S. Suslick, *Chem. Soc. Rev.*, 2013, **42**, 2555–2567.
55 G. Han, Y. Liu, E. Kan, J. Tang, L. Zhang, H. Wang and W. Tang, *RSC Adv.*, 2014, **4**, 9898–9904.
56 J. K. Gan, Y. S. Lim, N. M. Huang and H. N. Lim, *Appl. Surf. Sci.*, 2015, **357**, 479–486.
57 S. Sarkar, E. Guibal, F. Quignard and A. K. SenGupta, *J. Nanopart. Res.*, 2012, **14**(2), 1–24.
58 K. Liang, T. Gu, Z. Cao, X. Tang, W. Hu and B. Wei, *Nano Energy*, 2014, **9**, 245–251.
59 M. D. Ingram, H. Staesche and K. S. Ryder, *Solid State Ionics*, 2004, **169**, 51–57.
60 R. K. Sharma, A. C. Rastogi and S. B. Desu, *Electrochem. Commun.*, 2008, **10**, 268–272.
61 S. S. Shinde, G. S. Gund, V. S. Kumbhar, B. H. Patil and C. D. Lokhande, *Eur. Polym. J.*, 2013, **49**, 3734–3739.
62 A. Yavuz, N. Ozdemir and H. Zengin, *Int. J. Hydrogen Energy*, 2020, **45**, 18876–18887.
63 D. P. Dubal, S. V. Patil, W. B. Kim and C. D. Lokhande, *Mater. Lett.*, 2011, **65**, 2628–2631.
64 B. Gnana, S. Raj, A. M. Asiri, A. H. Qusti, J. J. Wu and S. Anandan, *Ultrason. Sonochem.*, 2014, **21**, 1933–1938.
65 G. Ali, M. Yusoff, Y. Ng, H. Lim and C. Feng, *Curr. Appl. Phys.*, 2015, **15**, 1143–1147.
66 A. H. P. De Oliveira, M. L. F. Nascimento and H. P. De Oliveira, *Mater. Res.*, 2016, **19**, 1080–1087.
67 L. Zhang, X. Peng, J. Wan, Q. Cui, X. Chu, H. Suo, C. Zhao and D. He, *Nano*, 2020, **15**, 1–9.
68 F. Grote and Y. Lei, *Nano Energy*, 2014, **10**, 63–70.
69 E. Karaca, D. Gökcen, N. Ö. Pekmez and K. Pekmez, *Electrochim. Acta*, 2019, **305**, 502–513.
70 X. Li, Y. Ma, P. Shen, C. Zhang, M. Cao, S. Xiao, J. Yan, S. Luo and Y. Gao, *Adv. Mater. Technol.*, 2020, **5**, 1–8.
71 Y. Li, H. Zhan, M. Wang, K. Liu and C. Yang, *2020 21st Int. Conf. Electron. Packag. Technol. ICEPT*, 2020, pp. 3–6.
72 T. G. Yun, B. Il Hwang, D. Kim, S. Hyun and S. M. Han, *ACS Appl. Mater. Interfaces*, 2015, **7**, 9228–9234.